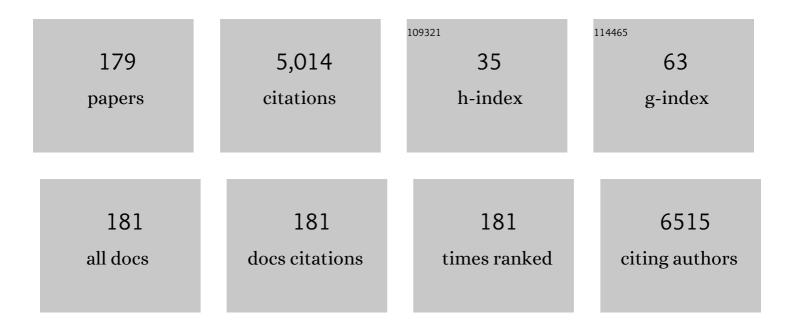
## Kohsuke Kudo

List of Publications by Year in descending order

Source: https://exaly.com/author-pdf/168265/publications.pdf Version: 2024-02-01



#	Article	IF	CITATIONS
1	Efficacy of Quantitative Susceptibility Mapping with Brain Surface Correction and Vein Removal for Detecting Increase Magnetic Susceptibility in Patients with Alzheimer's Disease. Magnetic Resonance in Medical Sciences, 2023, 22, 87-94.	2.0	4
2	Intraocular Water Movement Visualization Using <scp><sup>1</sup>Hâ€MRI</scp> With Eye Drops of Oâ€17â€Labeled Saline: Firstâ€inâ€Human Study. Journal of Magnetic Resonance Imaging, 2023, 57, 845-853.	3.4	6
3	Quantitative Susceptibility Mapping versus R2*-based Histogram Analysis for Evaluating Liver Fibrosis: Preliminary Results. Magnetic Resonance in Medical Sciences, 2022, 21, 609-622.	2.0	5
4	Quantitative magnetic resonance imaging for evaluating of the cerebrospinal fluid kinetics with 170-labeled water tracer: A preliminary report. Magnetic Resonance Imaging, 2022, 87, 77-85.	1.8	6
5	Development of three-dimensional MR neurography using an optimized combination of compressed sensing and parallel imaging. Magnetic Resonance Imaging, 2022, 87, 32-37.	1.8	7
6	Artificial intelligence for nuclear medicine in oncology. Annals of Nuclear Medicine, 2022, 36, 123-132.	2.2	12
7	DWI-related texture analysis for prostate cancer: differences in correlation with histological aggressiveness and data repeatability between peripheral and transition zones. European Radiology Experimental, 2022, 6, 1.	3.4	5
8	Single-Session Intranodal Glue Embolization for Postsurgical Refractory Groin Lymphorrhea: A Case Report. Interventional Radiology, 2022, 7, 30-33.	0.4	1
9	Penumbra Detection With Oxygen Extraction Fraction Using Magnetic Susceptibility in Patients With Acute Ischemic Stroke. Frontiers in Neurology, 2022, 13, 752450.	2.4	6
10	Increased Cerebral Small Vessel Disease Burden With Renal Dysfunction and Albuminuria in Patients Taking Antithrombotic Agents: The Bleeding With Antithrombotic Therapy 2. Journal of the American Heart Association, 2022, 11, e024749.	3.7	5
11	Phase I Randomized Trial of <scp><sup>17</sup>O</scp> â€Labeled Water: Safety and Feasibility Study of Indirect Proton <scp>MRI</scp> for the Evaluation of Cerebral Water Dynamics. Journal of Magnetic Resonance Imaging, 2022, 56, 1874-1882.	3.4	6
12	Quantitative Susceptibility Mapping: Basic Methods and Clinical Applications. Radiographics, 2022, 42, 1161-1176.	3.3	15
13	Imaging findings of ovarian metastasis of primary renal cell carcinoma: A case report and literature review. Radiology Case Reports, 2022, 17, 2320-2327.	0.6	0
14	18F-FMISO PET/CT detects hypoxic lesions of cardiac and extra-cardiac involvement in patients with sarcoidosis. Journal of Nuclear Cardiology, 2021, 28, 2141-2148.	2.1	23
15	Reinterpretation of magnetic resonance imaging findings with magnetoencephalography can improve the accuracy of detecting epileptogenic cortical lesions. Epilepsy and Behavior, 2021, 114, 107516.	1.7	2
16	Preliminary study of Al-assisted diagnosis using FDG-PET/CT for axillary lymph node metastasis in patients with breast cancer. EJNMMI Research, 2021, 11, 10.	2.5	20
17	Evaluation of oral air space volume in obstructive sleep apnea syndrome using clinical and postmortem CT imaging. Oral Radiology, 2021, , 1.	1.9	1
18	Evaluation of whole-body modalities for diagnosis of multifocal osteonecrosis—a pilot study. Arthritis Research and Therapy, 2021, 23, 83.	3.5	4

#	Article	IF	CITATIONS
19	Low <i>b</i> â€value diffusion tensor imaging for measuring pseudorandom flow of cerebrospinal fluid. Magnetic Resonance in Medicine, 2021, 86, 1369-1382.	3.0	15
20	Favorable Effects of Burosumab on Fibroblast Growth Factor 23-Related Osteomalacia: A Case Report. Journal of the Endocrine Society, 2021, 5, A194-A194.	0.2	0
21	4-Dimensional Flow Cardiovascular Magnetic Resonance Imaging of Changes in Blood Flow Dynamics After Surgery for Discrete Subaortic Stenosis. Circulation Journal, 2021, 85, 954.	1.6	0
22	Editorial for "Individualized Prediction of Early Alzheimer's Disease Based on <scp>MRI</scp> Radiomics, Clinical and Laboratory Examinations: A 60â€Month Followâ€up Study― Journal of Magnetic Resonance Imaging, 2021, 54, 1658-1659.	3.4	0
23	Extremely low <sup>18</sup> F-fluorodeoxyglucose uptake in the brain of a patient with metastatic neuroblastoma and its recovery after chemotherapy: A case report. Acta Radiologica Open, 2021, 10, 205846012110268.	0.6	2
24	Prediction of the local treatment outcome in patients with oropharyngeal squamous cell carcinoma using deep learning analysis of pretreatment FDG-PET images. BMC Cancer, 2021, 21, 900.	2.6	12
25	Development and validation of a prediction model based on the organ-based metabolic tumor volume on FDG-PET in patients with differentiated thyroid carcinoma. Annals of Nuclear Medicine, 2021, 35, 1223-1231.	2.2	7
26	Successful transvenous embolization for type II uterine arteriovenous malformation: A case report. Radiology Case Reports, 2021, 16, 2007-2011.	0.6	3
27	Association of high serum soluble interleukin 2 receptor levels with risk of adverse events in cardiac sarcoidosis. ESC Heart Failure, 2021, 8, 5282-5292.	3.1	11
28	Preoperative Texture Analysis Using 11C-Methionine Positron Emission Tomography Predicts Survival after Surgery for Glioma. Diagnostics, 2021, 11, 189.	2.6	4
29	Texture analysis of delayed contrast-enhanced computed tomography to diagnose cardiac sarcoidosis. Japanese Journal of Radiology, 2021, 39, 442-450.	2.4	7
30	Favorable effects of burosumab on tumor-induced osteomalacia caused by an undetectable tumor. Medicine (United States), 2021, 100, e27895.	1.0	6
31	Variations and natural history of primary intraparenchymal lesions associated with neurofibromatosis type 2. Neuroradiology, 2021, , 1.	2.2	0
32	Multiparametric Analysis of Tumor Morphological and Functional MR Parameters Potentially Predicts Local Failure in Pharynx Squamous Cell Carcinoma Patients. Journal of Medical Investigation, 2021, 68, 354-361.	0.5	1
33	Percutaneous insertion of hepatic fiducial true-spherical markers for real-time adaptive radiotherapy. Minimally Invasive Therapy and Allied Technologies, 2020, 29, 334-343.	1.2	8
34	Prediction of Hypoxia in Brain Tumors Using a Multivariate Model Built from MR Imaging and <sup>18</sup> F-Fluorodeoxyglucose Accumulation Data. Magnetic Resonance in Medical Sciences, 2020, 19, 227-234.	2.0	3
35	Influence of the scan time point when assessing hypoxia in 18F-fluoromisonidazole PET: 2 vs. 4Âh. European Journal of Nuclear Medicine and Molecular Imaging, 2020, 47, 1833-1842.	6.4	10
36	The bleeding with antithrombotic therapy study 2: Rationale, design, and baseline characteristics of the participants. European Stroke Journal, 2020, 5, 423-431.	5.5	3

#	Article	IF	CITATIONS
37	Visualization of Quantitative Flow Reduction with 4D-flow Magnetic Resonance Imaging in a Patient with Pelvic Arteriovenous Malformation After Transcatheter Arterial Embolization. CardioVascular and Interventional Radiology, 2020, 43, 1557-1560.	2.0	0
38	Improvement of image quality on low-dose dynamic myocardial perfusion computed tomography with a novel 4-dimensional similarity filter. Medicine (United States), 2020, 99, e20804.	1.0	8
39	Consensus survey on pre-procedural safety practices in radiological examinations: a multicenter study in seven Asian regions. British Journal of Radiology, 2020, 93, 20200082.	2.2	1
40	Correlation analysis between magnetic susceptibility in MRI and amyloid β in PET. Alzheimer's and Dementia, 2020, 16, e040064.	0.8	1
41	Utility of a diffusion-weighted arterial spin labeling (DW-ASL) technique for evaluating the progression of brain white matter lesions. Magnetic Resonance Imaging, 2020, 69, 81-87.	1.8	7
42	Microstructural Alterations in Bipolar and Major Depressive Disorders: A Diffusion Kurtosis Imaging Study. Journal of Magnetic Resonance Imaging, 2020, 52, 1187-1196.	3.4	7
43	Spontaneous rupture of the pancreatic arcade artery caused by neurofibromatosis type 1 successfully treated using emergency transcatheter arterial embolization, partial intra-aortic balloon occlusion, and stent graft placement: a case report and review of the literature. CVIR Endovascular, 2020, 3, 37.	1.1	3
44	Nationwide questionnaire survey on neuroimaging strategy for acute ischemic stroke in Japan. Nosotchu, 2020, 42, 502-508.	0.1	1
45	Acute cerebrovascular imaging for stroke management: a literature review. Nosotchu, 2020, 42, 495-501.	0.1	1
46	Halo artifacts of indwelling urinary catheter by inaccurate scatter correction in 18F-FDG PET/CT imaging: incidence, mechanism, and solutions. EJNMMI Physics, 2020, 7, 66.	2.7	4
47	Assessment of Coronary Flow Velocity Reserve in the Left Main Trunk Using Phase-contrast MR Imaging at 3T: Comparison with <sup>15</sup> O-labeled Water Positron Emission Tomography. Magnetic Resonance in Medical Sciences, 2019, 18, 134-141.	2.0	1
48	Detection of microbleeds associated with sentinel headache using MRI quantitative susceptibility mapping: pilot study. Journal of Neurosurgery, 2019, 130, 1391-1397.	1.6	15
49	Machine-Learning-Based Prediction of Treatment Outcomes Using MR Imaging-Derived Quantitative Tumor Information in Patients with Sinonasal Squamous Cell Carcinomas: A Preliminary Study. Cancers, 2019, 11, 800.	3.7	31
50	Magnetic resonance imaging T1 and T2 mapping provide complementary information on the bone mineral density regarding cancellous bone strength in the femoral head of postmenopausal women with osteoarthritis. Clinical Biomechanics, 2019, 65, 13-18.	1.2	8
51	Predicting metastasis in clinically negative axillary lymph nodes with minimum apparent diffusion coefficient value in luminal A-like breast cancer. Breast Cancer, 2019, 26, 628-636.	2.9	8
52	The utility of MRI histogram and texture analysis for the prediction of histological diagnosis in head and neck malignancies. Cancer Imaging, 2019, 19, 5.	2.8	57
53	ICâ€Pâ€139: A MULTICENTER STUDY OF THE CORRELATION BETWEEN THE QUANTITATIVE SUSCEPTIBILITY MAPF OF MAGNETIC RESONANCE IMAGING AND AMYLOID POSITRON EMISSION TOMOGRAPHY. Alzheimer's and Dementia, 2019, 15, P114.	PING 0.8	0
54	Three-dimensional Pseudo-continuous Arterial Spin-labeling Using Turbo-spin Echo with Pseudo-steady State Readout: A Comparison with Other Major Readout Methods. Magnetic Resonance in Medical Sciences, 2019, 18, 170-177.	2.0	4

#	Article	IF	CITATIONS
55	Evaluation of oxygen extraction fraction in systemic lupus erythematosus patients using quantitative susceptibility mapping. Journal of Cerebral Blood Flow and Metabolism, 2019, 39, 1648-1658.	4.3	8
56	Quantitative Evaluation of Myocardial Ischemia with Dynamic Perfusion CT. Annals of Nuclear Cardiology, 2019, 5, 79-83.	0.2	1
57	Automatic metastatic bone tumor classification with DCNN-based features using treatment-planning CT. , 2019, , .		0
58	Phase I study of <sup>17</sup> O-labeled water : safety and feasibility study of indirect proton MRI for the evaluation of cerebral blood flow [Presidential Award Proceedings]. Japanese Journal of Magnetic Resonance in Medicine, 2019, 39, 66.	0.0	0
59	Indirect MRI of <sup>17</sup> oâ€labeled water using steadyâ€state sequences: Signal simulation and preclinical experiment. Journal of Magnetic Resonance Imaging, 2018, 47, 1373-1379.	3.4	13
60	Improvement of the repeatability of parallel transmission at 7T using interleaved acquisition in the calibration scan. Journal of Magnetic Resonance Imaging, 2018, 48, 94-101.	3.4	5
61	Accelerating Cell Therapy for Stroke in Japan. Stroke, 2018, 49, e145-e152.	2.0	10
62	Noninvasive electrical conductivity measurement by MRI: a test of its validity and the electrical conductivity characteristics of glioma. European Radiology, 2018, 28, 348-355.	4.5	68
63	Heterogeneity of longitudinal and circumferential contraction in relation to late gadolinium enhancement in hypertrophic cardiomyopathy patients with preserved left ventricular ejection fraction. Japanese Journal of Radiology, 2018, 36, 103-112.	2.4	6
64	Simple modification of arm position improves B <sub>1</sub> <sup>+</sup> and signal homogeneity in the thoracolumbar spine at 3T. Journal of Magnetic Resonance Imaging, 2018, 47, 123-130.	3.4	3
65	ICâ€Pâ€188: HYBRID SEQUENCE AND ANALYSIS OF T1â€WEIGHTED IMAGING AND QUANTITATIVE SUSCEPTIBILI MAPPING FOR EARLY DIAGNOSIS OF ALZHEIMER'S DISEASE. Alzheimer's and Dementia, 2018, 14, P156.	ΓΥ <sub>0.8</sub>	0
66	P2â€388: DETECTION OF INCREASED MAGNETIC SUSCEPTIBILITIES IN THE CEREBRAL CORTEX IN PATIENTS WITH ALZHEIMER'S DISEASE: COMPARISON OF QUANTITATIVE SUSCEPTIBILITY MAPPING BETWEEN CONVENTIONAL AND BRAIN SURFACE CORRECTION METHOD. Alzheimer's and Dementia, 2018, 14, P848.	0.8	0
67	P2â€384: HYBRID SEQUENCE AND ANALYSIS OF T1â€WEIGHTED IMAGING AND QUANTITATIVE SUSCEPTIBILITY MAPPING FOR EARLY DIAGNOSIS OF ALZHEIMER'S DISEASES. Alzheimer's and Dementia, 2018, 14, P845.	0.8	1
68	Semi-quantitative analysis of pre-treatment morphological and intratumoral characteristics using 18F-fluorodeoxyglucose positron-emission tomography as predictors of treatment outcome in nasal and paranasal squamous cell carcinoma. Quantitative Imaging in Medicine and Surgery, 2018, 8, 788-795.	2.0	10
69	ICâ€Pâ€194: DETECTION OF INCREASED MAGNETIC SUSCEPTIBILITIES IN THE CEREBRAL CORTEX IN PATIENTS W ALZHEIMER'S DISEASE: COMPARISON OF QUANTITATIVE SUSCEPTIBILITY MAPPING BETWEEN CONVENTIONAL AND BRAIN SURFACE CORRECTION METHOD. Alzheimer's and Dementia, 2018, 14, P160.	'ITH 0.8	1
70	lgG4-related Cardiovascular Disease from the Aorta to the Coronary Arteries: Multidetector CT and PET/CT. Radiographics, 2018, 38, 1934-1948.	3.3	60
71	Indirect Proton MR Imaging and Kinetic Analysis of <sup>17</sup> O-Labeled Water Tracer in the Brain. Magnetic Resonance in Medical Sciences, 2018, 17, 223-230.	2.0	26
72	Utility of a Hybrid IVIM-DKI Model to Predict the Development of Distant Metastasis in Head and Neck Squamous Cell Carcinoma Patients. Magnetic Resonance in Medical Sciences, 2018, 17, 21-27.	2.0	15

#	Article	IF	CITATIONS
73	Spontaneous Recovery of Multiple Hepatic Artery Aneurysms with Segmental Arterial Mediolysis. Interventional Radiology, 2018, 3, 88-92.	0.4	0
74	Prediction of the treatment outcome using intravoxel incoherent motion and diffusional kurtosis imaging in nasal or sinonasal squamous cell carcinoma patients. European Radiology, 2017, 27, 956-965.	4.5	48
75	Characteristics of immunoglobulin G4-related aortitis/periaortitis and periarteritis on fluorodeoxyglucose positron emission tomography/computed tomography co-registered with contrast-enhanced computed tomography. EJNMMI Research, 2017, 7, 20.	2.5	57
76	The Steerable Microcatheter: A New Device for Selective Catheterisation. CardioVascular and Interventional Radiology, 2017, 40, 947-952.	2.0	38
77	Delayed contrast-enhanced computed tomography in patients with known or suspected cardiac sarcoidosis: A feasibility study. European Radiology, 2017, 27, 4054-4063.	4.5	36
78	Residual tumour detection in post-treatment granulation tissue by using advanced diffusion models in head and neck squamous cell carcinoma patients. European Journal of Radiology, 2017, 90, 14-19.	2.6	6
79	Advanced diffusion models in head and neck squamous cell carcinoma patients: Goodness of fit, relationships among diffusion parameters and comparison with dynamic contrast-enhanced perfusion. Magnetic Resonance Imaging, 2017, 36, 16-23.	1.8	33
80	Preoperative Cerebral Oxygen Extraction Fraction Imaging Generated from 7T MR Quantitative Susceptibility Mapping Predicts Development of Cerebral Hyperperfusion following Carotid Endarterectomy. American Journal of Neuroradiology, 2017, 38, 2327-2333.	2.4	6
81	Fast acceleration of ASL-based time-resolved magnetic resonance angiography by acquisition of control and labeled images in the same shot (fast ACTRESS): An optimization study. Magnetic Resonance Imaging, 2017, 43, 136-143.	1.8	0
82	Noninvasive Assessment of Oxygen Extraction Fraction in Chronic Ischemia Using Quantitative Susceptibility Mapping at 7 Tesla. Stroke, 2017, 48, 2136-2141.	2.0	38
83	Tmax Determined Using a Bayesian Estimation Deconvolution Algorithm Applied to Bolus Tracking Perfusion Imaging: A Digital Phantom Validation Study. Magnetic Resonance in Medical Sciences, 2017, 16, 32-37.	2.0	1
84	Comparison of Different Post-Processing Algorithms for Dynamic Susceptibility Contrast Perfusion Imaging of Cerebral Gliomas. Magnetic Resonance in Medical Sciences, 2017, 16, 129-136.	2.0	9
85	Non-invasive prediction of the tumor growth rate using advanced diffusion models in head and neck squamous cell carcinoma patients. Oncotarget, 2017, 8, 33631-33643.	1.8	5
86	Breath-holding during the Calibration Scan Improves the Reproducibility of Parallel Transmission at 7T for Human Brain. Magnetic Resonance in Medical Sciences, 2017, 16, 23-31.	2.0	6
87	Feasibility and Efficiency of Human Bone Marrow Stromal Cell Culture with Allogeneic Platelet Lysate-Supplementation for Cell Therapy against Stroke. Stem Cells International, 2016, 2016, 1-11.	2.5	15
88	Optimization of Scan Parameters to Reduce Acquisition Time for Diffusion Kurtosis Imaging at 1.5T. Magnetic Resonance in Medical Sciences, 2016, 15, 41-48.	2.0	23
89	Fast nonlinear regression method for CT brain perfusion analysis. Journal of Medical Imaging, 2016, 3, 026003.	1.5	14
90	Usefulness of Pseudocontinuous Arterial Spin-Labeling for the Assessment of Patients with Head and Neck Squamous Cell Carcinoma by Measuring Tumor Blood Flow in the Pretreatment and Early Treatment Period. American Journal of Neuroradiology, 2016, 37, 342-348.	2.4	29

#	Article	IF	CITATIONS
91	Comparison of conventional ultrasonography and ultrasonography-computed tomography fusion imaging for target identification using digital/real hybrid phantoms: a preliminary study. Journal of Medical Ultrasonics (2001), 2016, 43, 327-335.	1.3	0
92	Evaluation of diagnostic accuracy in CT perfusion analysis in moyamoya disease. Japanese Journal of Radiology, 2016, 34, 28-34.	2.4	1
93	Utility of noncontrastâ€enhanced timeâ€resolved fourâ€dimensional MR angiography with a vesselâ€selective technique for intracranial arteriovenous malformations. Journal of Magnetic Resonance Imaging, 2016, 44, 834-845.	3.4	24
94	Differences in morphological features and minimum apparent diffusion coefficient values among breast cancer subtypes using 3-tesla MRI. European Journal of Radiology, 2016, 85, 96-102.	2.6	30
95	Comparison between borderline ovarian tumors and carcinomas using semi-automated histogram analysis of diffusion-weighted imaging: focusing on solid components. Japanese Journal of Radiology, 2016, 34, 229-237.	2.4	23
96	Prognostic Imaging Biomarkers in Glioblastoma: Development and Independent Validation on the Basis of Multiregion and Quantitative Analysis of MR Images. Radiology, 2016, 278, 546-553.	7.3	90
97	Oxygen extraction fraction measurement using quantitative susceptibility mapping: Comparison with positron emission tomography. Journal of Cerebral Blood Flow and Metabolism, 2016, 36, 1424-1433.	4.3	82
98	Glucose Metabolism and Its Complicated Relationship with Tumor Growth and Perfusion in Head and Neck Squamous Cell Carcinoma. PLoS ONE, 2016, 11, e0166236.	2.5	6
99	Observational cohort study of first-line bevacizumab with oxaliplatin or irinotecan and fluoropyrimidines in metastatic colorectal cancer: HGCSG0802—Analysis of early tumor shrinkage (ETS) Journal of Clinical Oncology, 2016, 34, 753-753.	1.6	0
100	International Survey of Acute Stroke Imaging Used to Make Revascularization Treatment Decisions. International Journal of Stroke, 2015, 10, 759-762.	5.9	50
101	Susceptibilityâ€Weighted Phase Imaging and Oxygen Extraction Fraction Measurement during Sedation and Sedation Recovery using 7T MRI. Journal of Neuroimaging, 2015, 25, 575-581.	2.0	10
102	Five-point Likert scaling on MRI predicts clinically significant prostate carcinoma. BMC Urology, 2015, 15, 91.	1.4	29
103	Quantification of myocardial blood flow with dynamic perfusion 3.0 Tesla MRI: Validation with <sup>15</sup> oâ€water PET. Journal of Magnetic Resonance Imaging, 2015, 42, 754-762.	3.4	29
104	Assessment of Sensations Experienced by Subjects during MR Imaging Examination at 7T. Magnetic Resonance in Medical Sciences, 2015, 14, 35-41.	2.0	11
105	Prediction of pancreatic anastomotic failure after pancreatic head resection using preoperative diffusion-weighted MR imaging. Japanese Journal of Radiology, 2015, 33, 59-66.	2.4	5
106	Diagnostic value of tumor blood flow and its histogram analysis obtained with pCASL to differentiate sinonasal malignant lymphoma from squamous cell carcinoma. European Journal of Radiology, 2015, 84, 2187-2193.	2.6	20
107	Transcatheter Arterial Embolization with Ethanol Injection in Symptomatic Patients with Enlarged Polycystic Kidneys. Radiology, 2015, 277, 277-285.	7.3	13
108	Detection of early changes in the parahippocampal and posterior cingulum bundles during mild cognitive impairment by using high-resolution multi-parametric diffusion tensor imaging. Psychiatry Research - Neuroimaging, 2015, 231, 346-352.	1.8	21

#	Article	IF	CITATIONS
109	Evaluation of cerebral blood flow using multi-phase pseudo continuous arterial spin labeling at 3-tesla. Magnetic Resonance Imaging, 2015, 33, 1338-1344.	1.8	7
110	Measurement of tumor blood flow in head and neck squamous cell carcinoma by pseudo ontinuous arterial spin labeling: Comparison with dynamic contrastâ€enhanced MRI. Journal of Magnetic Resonance Imaging, 2015, 41, 983-991.	3.4	45
111	Use of transabdominal ultrasonography to preoperatively determine T-stage of proven colon cancers. Abdominal Imaging, 2015, 40, 1441-1450.	2.0	6
112	Detection of changes in the locus coeruleus in patients with mild cognitive impairment and <scp>A</scp> lzheimer's disease: Highâ€resolution fast spinâ€echo <scp>T</scp> 1â€weighted imaging. Geriatrics and Gerontology International, 2015, 15, 334-340.	1.5	76
113	Identifying Triple-Negative Breast Cancer Using Background Parenchymal Enhancement Heterogeneity on Dynamic Contrast-Enhanced MRI: A Pilot Radiomics Study. PLoS ONE, 2015, 10, e0143308.	2.5	110
114	Association of early tumor shrinkage with progression-free survival in patients with metastatic colorectal cancer treated with bevacizumab-based chemotherapy: HGCSG0802 Journal of Clinical Oncology, 2015, 33, 749-749.	1.6	34
115	Association of morphologic response with progression free survival in patients with metastatic colorectal cancer treated with bevacizumab-based chemotherapy: HGCSG0802 Journal of Clinical Oncology, 2015, 33, 743-743.	1.6	Ο
116	Bayesian Analysis of Perfusion-weighted Imaging to Predict Infarct Volume: Comparison with Singular Value Decomposition. Magnetic Resonance in Medical Sciences, 2014, 13, 45-50.	2.0	22
117	Voxelâ€Based Morphometry of Disproportionate Cerebrospinal Fluid Space Distribution for the Differential Diagnosis of Idiopathic Normal Pressure Hydrocephalus. Journal of Neuroimaging, 2014, 24, 359-365.	2.0	21
118	Intensity inhomogeneity correction for magnetic resonance imaging of human brain at 7T. Medical Physics, 2014, 41, 022302.	3.0	28
119	Standardized Uptake Value in High Uptake Area on Positron Emission Tomography with 18F-FRP170 as a Hypoxic Cell Tracer Correlates with Intratumoral Oxygen Pressure in Glioblastoma. Molecular Imaging and Biology, 2014, 16, 127-135.	2.6	23
120	Altered magnetic resonance images of brain and social behaviors of hatchling, and expression of thyroid hormone receptor βmRNA in cerebellum of embryos after Methimazole administration. Psychopharmacology, 2014, 231, 221-230.	3.1	6
121	Intravoxel incoherent motion diffusion-weighted imaging in head and neck squamous cell carcinoma: Assessment of perfusion-related parameters compared to dynamic contrast-enhanced MRI. Magnetic Resonance Imaging, 2014, 32, 1206-1213.	1.8	69
122	Arterial spin labeling to determine tumor viability in head and neck cancer before and after treatment. Journal of Magnetic Resonance Imaging, 2014, 40, 920-928.	3.4	40
123	Quantification of myocardial blood flow using dynamic 320-row multi-detector CT as compared with 150-H2O PET. European Radiology, 2014, 24, 1547-1556.	4.5	87
124	Evaluating Middle Cerebral Artery Atherosclerotic Lesions in Acute Ischemic Stroke Using Magnetic Resonance T1-weighted 3-Dimensional Vessel Wall Imaging. Journal of Stroke and Cerebrovascular Diseases, 2014, 23, 706-711.	1.6	36
125	Noninvasive Evaluation of Collateral Blood Flow through Circle of Willis in Cervical Carotid Stenosis Using Selective Magnetic Resonance Angiography. Journal of Stroke and Cerebrovascular Diseases, 2014, 23, 1019-1023.	1.6	17
126	Assessment of the accuracy of a Bayesian estimation algorithm for perfusion CT by using a digital phantom. Neuroradiology, 2013, 55, 1197-1203.	2.2	26

#	Article	IF	CITATIONS
127	3D neuromelanin-sensitive magnetic resonance imaging with semi-automated volume measurement of the substantia nigra pars compacta for diagnosis of Parkinson's disease. Neuroradiology, 2013, 55, 719-724.	2.2	107
128	Penumbral Imaging by Using Perfusion Computed Tomography and Perfusion-Weighted Magnetic Resonance Imaging: Current Concepts. Journal of Stroke and Cerebrovascular Diseases, 2013, 22, 1212-1215.	1.6	7
129	The strain-encoded (SENC) MR imaging for detection of global right ventricular dysfunction in pulmonary hypertension. International Journal of Cardiovascular Imaging, 2013, 29, 371-378.	1.5	20
130	Changes in substantia nigra and locus coeruleus in patients with early-stage Parkinson's disease using neuromelanin-sensitive MR imaging. Neuroscience Letters, 2013, 541, 93-98.	2.1	144
131	Acute Stroke Imaging Research Roadmap II. Stroke, 2013, 44, 2628-2639.	2.0	192
132	Accuracy and Reliability Assessment of CT and MR Perfusion Analysis Software Using a Digital Phantom. Radiology, 2013, 267, 201-211.	7.3	131
133	Diffusion Anisotropy Colorâ€Coded Map of Cerebral White Matter: Quantitative Comparison between Orthogonal Anisotropic Diffusionâ€Weighted Imaging and Diffusion Tensor Imaging. Journal of Neuroimaging, 2013, 23, 197-201.	2.0	3
134	International Survey of Acute Stroke Imaging Capabilities. Stroke, 2013, 44, 2091-2091.	2.0	5
135	Postoperative Increase in Cerebral White Matter Fractional Anisotropy on Diffusion Tensor Magnetic Resonance Imaging Is Associated With Cognitive Improvement After Uncomplicated Carotid Endarterectomy. Neurosurgery, 2013, 73, 592-599.	1.1	32
136	Neuromelanin Imaging in Parkinson Disease. , 2013, , 159-164.		2
137	The alphabet soup of perfusion CT and MR imaging: terminology revisited and clarified in five questions. Neuroradiology, 2012, 54, 907-918.	2.2	25
138	Postoperative Cerebral White Matter Damage Associated with Cerebral Hyperperfusion and Cognitive Impairment after Carotid Endarterectomy: A Diffusion Tensor Magnetic Resonance Imaging Study. Cerebrovascular Diseases, 2012, 34, 358-367.	1.7	44
139	Two cases of spontaneous epidural emphysema during asthmatic attack. Respiratory Investigation, 2012, 50, 62-65.	1.8	4
140	Carotid plaque signal differences among four kinds of T1-weighted magnetic resonance imaging techniques: A histopathological correlation study. Neuroradiology, 2012, 54, 1187-1194.	2.2	44
141	Quantitative assessment of changes in carotid plaques during cilostazol administration using three-dimensional ultrasonography and non-gated magnetic resonance plaque imaging. Neuroradiology, 2012, 54, 939-945.	2.2	18
142	Visualization of the Superparamagnetic Iron Oxide (SPIO)-Labeled Bone Marrow Stromal Cells Using a 3.0-T MRI—a Pilot Study for Clinical Testing of Neurotransplantation. Translational Stroke Research, 2012, 3, 99-106.	4.2	13
143	CT and MR perfusion can discriminate severe cerebral hypoperfusion from perfusion absence: evaluation of different commercial software packages by using digital phantoms. Neuroradiology, 2012, 54, 467-474.	2.2	15
144	Detecting damaged regions of cerebral white matter in the subacute phase after carbon monoxide poisoning using voxel-based analysis with diffusion tensor imaging. Neuroradiology, 2012, 54, 681-689.	2.2	21

#	Article	IF	CITATIONS
145	Proton Magnetic Resonance Spectroscopic Images in Preterm Infants with Bilirubin Encephalopathy. Journal of Pediatrics, 2012, 160, 342-344.	1.8	11
146	Non-invasive measurement of oxygen saturation in the spinal vein using SWI: Quantitative evaluation under conditions of physiological and caffeine load. NeuroImage, 2011, 54, 344-349.	4.2	16
147	Detection of Active Plaques in Multiple Sclerosis using Susceptibility-weighted Imaging: Comparison with Gadolinium-enhanced MR Imaging. Magnetic Resonance in Medical Sciences, 2011, 10, 185-192.	2.0	10
148	High-resolution Diffusion Tensor Imaging for the Detection of Diffusion Abnormalities in the Trigeminal Nerves of Patients with Trigeminal Neuralgia Caused by Neurovascular Compression. , 2011, 21, e102-e108.		62
149	Prediction of Infarct Volume and Neurologic Outcome by using Automated Multiparametric Perfusion-Weighted Magnetic Resonance Imaging in a Primate Model of Permanent Middle Cerebral Artery Occlusion. Journal of Cerebral Blood Flow and Metabolism, 2011, 31, 448-456.	4.3	20
150	Susceptibility of Tmax to Tracer Delay on Perfusion Analysis: Quantitative Evaluation of Various Deconvolution Algorithms Using Digital Phantoms. Journal of Cerebral Blood Flow and Metabolism, 2011, 31, 908-912.	4.3	33
151	Identification and further differentiation of subendocardial and transmural myocardial infarction by fast strain-encoded (SENC) magnetic resonance imaging at 3.0 Tesla. European Radiology, 2011, 21, 2362-2368.	4.5	42
152	Prediction of malignancy grading using computed tomography perfusion imaging in nonenhancing supratentorial gliomas. Journal of Neuro-Oncology, 2011, 103, 619-627.	2.9	10
153	Mapping of Cerebral Oxygen Extraction Fraction Changes with Susceptibility-weighted Phase Imaging. Radiology, 2011, 261, 930-936.	7.3	39
154	Susceptibility-weighted Imaging and Magnetic Resonance Angiography during Migraine Attack: A Case Report. Magnetic Resonance in Medical Sciences, 2011, 10, 49-52.	2.0	14
155	Susceptibility-Weighted Imaging of Cerebral Fat Embolism. Journal of Computer Assisted Tomography, 2010, 34, 107-112.	0.9	35
156	Visual discrimination among patients with depression and schizophrenia and healthy individuals using semiquantitative color-coded fast spin-echo T1-weighted magnetic resonance imaging. Neuroradiology, 2010, 52, 83-89.	2.2	24
157	Detection of changes in cerebrospinal fluid space in idiopathic normal pressure hydrocephalus using voxel-based morphometry. Neuroradiology, 2010, 52, 381-386.	2.2	42
158	Detection of normal spinal veins by using susceptibilityâ€weighted imaging. Journal of Magnetic Resonance Imaging, 2010, 31, 32-38.	3.4	21
159	Microstructural White Matter Abnormalities of Multiple System Atrophy: In Vivo Topographic Illustration by Using Diffusion-Tensor MR Imaging. Radiology, 2010, 255, 563-569.	7.3	51
160	Spinal Arteriovenous Malformation: Evaluation of Change in Venous Oxygenation with Susceptibility-weighted MR Imaging after Treatment. Radiology, 2010, 254, 891-899.	7.3	18
161	Brain Temperature Measured by Using Proton MR Spectroscopy Predicts Cerebral Hyperperfusion after Carotid Endarterectomy. Radiology, 2010, 256, 924-931.	7.3	20
162	Differences in CT Perfusion Maps Generated by Different Commercial Software: Quantitative Analysis by Using Identical Source Data of Acute Stroke Patients. Radiology, 2010, 254, 200-209.	7.3	292

#	Article	IF	CITATIONS
163	Difference in Tracer Delay–induced Effect among Deconvolution Algorithms in CT Perfusion Analysis: Quantitative Evaluation with Digital Phantoms. Radiology, 2009, 251, 241-249.	7.3	97
164	Prospective study on the mismatch concept in acute stroke patients within the first 24 h after symptom onset - 1000Plus study. BMC Neurology, 2009, 9, 60.	1.8	82
165	Susceptibility-Weighted Magnetic Resonance Imaging Detects Impaired Cerebral Hemodynamics in the Superior Sagittal Sinus Thrombosis -Case Report Neurologia Medico-Chirurgica, 2009, 49, 248-251.	2.2	18
166	Neuromelanin-Sensitive MRI. Klinische Neuroradiologie, 2008, 18, 147-153.	0.9	45
167	Realization of reliable cerebral-blood-flow maps from low-dose CT perfusion images by statistical noise reduction using nonlinear diffusion filtering. Radiological Physics and Technology, 2008, 1, 62-74.	1.9	23
168	MR susceptibility weighted imaging (SWI) complements conventional contrast enhanced T1 weighted MRI in characterizing brain abnormalities of Sturgeâ€Weber Syndrome. Journal of Magnetic Resonance Imaging, 2008, 28, 300-307.	3.4	89
169	Monoamine neurons in the human brain stem: anatomy, magnetic resonance imaging findings, and clinical implications. NeuroReport, 2008, 19, 1649-1654.	1.2	60
170	Contrast-enhanced FLAIR imaging in combination with pre- and postcontrast magnetization transfer T1-weighted imaging: Usefulness in the evaluation of brain metastases. Journal of Magnetic Resonance Imaging, 2007, 25, 479-487.	3.4	25
171	CT perfusion for acute stroke: Current concepts on technical aspects and clinical applications. International Congress Series, 2006, 1290, 30-36.	0.2	17
172	Early Detection of Subacute Sclerosing Panencephalitis by High b-Value Diffusion-Weighted Imaging. Journal of Computer Assisted Tomography, 2006, 30, 126-130.	0.9	3
173	Capillary Telangiectasia of the Brain Stem Diagnosed by Susceptibility-Weighted Imaging. Journal of Computer Assisted Tomography, 2006, 30, 980-982.	0.9	36
174	The role of tumor lysis in reversible posterior leukoencephalopathy syndrome. Pediatric Radiology, 2005, 35, 722-727.	2.0	25
175	Early detection of global cerebral anoxia: improved accuracy by high-b-value diffusion-weighted imaging with long echo time. American Journal of Neuroradiology, 2005, 26, 1487-97.	2.4	23
176	CT angiography with multidetector-row helical CT in spinal arteriovenous malformation. Clinical Imaging, 2004, 28, 23-27.	1.5	18
177	Physiologic change in flow velocity and direction of dural venous sinuses with respiration: MR venography and flow analysis. American Journal of Neuroradiology, 2004, 25, 551-7.	2.4	40
178	Quantitative cerebral blood flow measurement with dynamic perfusion CT using the vascular-pixel elimination method: comparison with H2(15)O positron emission tomography. American Journal of Neuroradiology, 2003, 24, 419-26.	2.4	158
179	Physical aspects of a real-time tumor-tracking system for gated radiotherapy. International Journal of Radiation Oncology Biology Physics, 2000, 48, 1187-1195.	0.8	603